Journal of Computational and Applied Mathematics 374 (2020) 112714

Contents lists available at ScienceDirect

Journal of Computational and Applied Mathematics

journal homepage: www.elsevier.com/locate/cam

A note on the adaptive numerical solution of a Riemann–Liouville space-fractional Kawarada problem

Lin Zhu [a,*,1], Qin Sheng [b,2]

[a] School of Mathematics and Statistics, Ningxia University, Yinchuan 750021, China
[b] Department of Mathematics and Center for Astrophysics, Space Physics and Engineering Research, Baylor University, Waco, TX 76798-7328, USA

ARTICLE INFO

Article history:
Received 26 June 2019
Received in revised form 11 November 2019

Keywords:
Fractional Kawarada problem
Positivity
Monotonicity
Critical length
Quenching time
Quenching location

ABSTRACT

This paper concerns the approximation and numerical solution of a singular fractional reaction–diffusion problem. A Riemann–Liouville space-fractional derivative oriented Laplacian is incorporated. While our spatial discretization is fulfilled though combined standard and shifted Grünwald formulas, temporal integration is accomplished via an implicit adaptive Crank–Nicolson scheme. It is proven that under proper constraints of the spatial and temporal discretization parameters, the numerical procedure implemented is positive, monotone and numerically stable. Simulation experiments are given to validate correlations between the fractional derivative and critical values including critical lengths, quenching times and locations.

© 2020 Published by Elsevier B.V.

1. Introduction

Nonlinear reaction–diffusion equations of the quenching type have been essential to simulation of thermal phenomena such as fuel combustion, energy transformation, cell multiplication and oil pipeline decay preventions [1–5]. Different from conventional blow-up problems, solutions of quenching partial differential equation problems remain to be bounded, while their rates of changes tend to be unbounded as quenching-combustion takes place. This introduces significant amounts of difficulties in modeling and computations of the quenching solutions [2,6–8].

To commence, we denote $\Omega_a = (0, a)$. Consider the following typical quenching-combustion problem:

$$u_t(x,t) = u_{xx}(x,t) + f(u), \quad x \in \Omega_a,\ 0 < t < T, \tag{1.1}$$

$$u(0,t) = u(a,t) = 0, \quad 0 \le t < T, \tag{1.2}$$

$$u(x,0) = \phi(x), \quad x \in \Omega_a, \tag{1.3}$$

where $f(u) = 1/(1-u)^\theta$, $\theta > 0$, $\phi \in C(\Omega_a)$ with $0 \le \phi \ll 1$ for $T \le \infty$. This spatially localized model describes a steady combustion process in which two gases meet in a gap between porous walls at distance a apart. Fuel diffusions on one wall. On the other hand, oxidant is at the other side dying out towards each wall and there is a reaction zone between two walls. Here t is the time, x is the distance between two walls and u is the temperature of uniform scaling [9].

* Corresponding author.
E-mail addresses: zhul@nxu.edu.cn (L. Zhu), qin_sheng@baylor.edu (Q. Sheng).

1 This author is supported in part by an NSF China/Ningxia research grant (No. 2018AAC03026).

2 This author is supported in part by an American Mathematics Society grant, in the form of FAN Award (AMS-F-32180177), and a NSF China research grant (No. 11772165).

https://doi.org/10.1016/j.cam.2020.112714
0377-0427/© 2020 Published by Elsevier B.V.

Further, θ is the physical property index of the gas involved. In 1975, Kawarada discovered that for $\theta = 1$, there exists a critical number $a^\star > 0$ such that if $a < a^\star$, the solution of Eqs. (1.1)–(1.3) exists globally [10]. Otherwise, there exists a finite time $T_a^\star$ such that $\lim_{t\to T_a^{\star-}} \sup_x u(x,t) = 1$. Herewith $a^\star$ is referred to as the critical length of domain and $T_a^\star$ is the critical time. It has also been reported that the problem (1.1)–(1.3) can be nonlocalized in electrostatic applications [11]. The solution of (1.1)–(1.3) is called to quench at $T_a^\star$ in the latter case [1,10].

To predict aforementioned quenching criterion, location of initial quench and influence of stochastic interferences has been a key to not only a better understanding of the thermal phenomena, but also designing and manufacturing of highly effective combustion processes in applications. Researchers have initially focused on theoretical estimates of critical values of different quenching processes [5,6,10]. Karawada observed that $a^\star > 2\sqrt{2}$ [10]. Later, Acker and Walter improved this to $a^\star \approx 1.5303$ [1]. Most existing results are acquired through discussions via reduced differential equations $u_{xx} = -f(u),\ 0 < x < a$, together with (1.2). Numerical methods such as boundary element and finite difference methods are popular for the numerical solution of (1.1)–(1.3) [4,6]. The computations, however, become significantly complicated as higher dimensional problems are concerned. To improve the accuracy and efficiency, adaptive strategies are introduced used for quenching problems [12]. Sophisticated splitting and domain decomposition methods are also considered [2,13]. To reduce the algorithmic complexity, methods of lines, or semidiscretizations, become a general rule in many numerical approaches. But this introduces other serious concerns such as the numerical instability. To break the barrier and obtain more accurate, reliable and straightforward computational strategies, applications of naturally endorsed and spatially global Kawarada model equations have become necessary.

Fractional partial differential equations (FPDEs) are generalizations of integral partial differential equations. The global feature of FPDEs has made them extremely important to applications where global effects are not neglectable. Natural phenomena targeted include heat diffusion, wave propagation, quantum mechanics, financial engineering, generic memory designs, electrochemistry and materials with complex rheological properties [14]. In this paper, we are particularly interested in FPDEs such as that when the Laplacian in (1.1) is replaced by the nonlocal α-fractional derivative for $1 < \alpha \le 2$. A few interesting theoretical and numerical explorations of such problems can be found in recent publications. For instance, Padgett considered possible quenching solutions to Kawarada problems when Caputo time-fractional derivatives are utilized [7]. Beauregard investigated quenching solutions of one-dimensional degenerate Kawarada problems equipped with left and right Riemann–Liouville fractional Laplacians [9]. It is found that fractional quenching models may preserve key global properties of the combustion environments and thus provide more realistic formulations for industrial simulations [7,15]. It has also been observed that orders of the fractional derivative have little influences on quenching locations while the degeneracy and transport coefficients play a significant role in the locations and quenching times. In our study, we will primarily focus on one-sided spatially fractional Kawarada problems and computations. Possible connections between orders of the fractional derivatives and critical values such as critical length, quenching time and quenching location will be explored.

The rest of the paper will be organized as follows. In Section 2, the spatially fractional model problem will be introduced and discussed. The fractional derivative is then approximated via a weighted Grünwald formula with a second order accuracy in the space [16]. The space fractional quenching singularity incurred will be handled through the semidiscretization and proper fractional approximations. Section 3 is devoted to the positivity and monotonicity of the numerical solution sequence generated by the semi-adaptive finite difference scheme. Rigorous numerical analysis and proof will be given on the stability of the fully discretized system. Numerical experiments will be presented in Section 4 to illustrate the solution of our fractional modeling problem. Important quenching properties related to our one dimensional fractional Kawarada equations will be demonstrated. Finally, in Section 5, conclusions will be given and highlighted. Continuing explorations will also be planned.

2. Fractional model and semi-adaptive scheme

Let $1 < \alpha \le 2$. For $T \le \infty$, we consider the following one-dimensional αth order nonlinear fractional initial–boundary value problem:

$$\frac{\partial u(x,t)}{\partial t} = d(x,t)\frac{\partial^\alpha u(x,t)}{\partial x^\alpha} + f(u), \quad x \in \Omega_a,\ 0 < t < T, \tag{2.1}$$

$$u(0,t) = u(a,t) = 0, \quad 0 \le t < T, \tag{2.2}$$

$$u(x,0) = \phi(x), \quad x \in \Omega_a, \tag{2.3}$$

where $f(u) = 1/(1-u),\ d(x,t) > 0$ for $x \in \Omega_a,\ 0 < t < T$. The problem provides a profound mathematical model for several physical and natural applications [17,18].

Let $x \in \Omega_a$ and $h = x/M$ for $M \in \mathbb{Z}^+$. We have following standard and shifted Grünwald formulas for the fractional derivative in (2.1), respectively [18]:

$$\frac{\partial^\alpha u(x,t)}{\partial x^\alpha} = \lim_{h\to 0^+} \frac{1}{h^\alpha} \sum_{m=0}^{M} g_m u(x - mh, t);$$

$$\frac{\partial^\alpha u(x,t)}{\partial x^\alpha} = \lim_{h\to 0^+}\frac{1}{h^\alpha}\sum_{m=0}^{M} g_m u(x-(m-1)h,t),$$

where

$$g_m = \frac{\Gamma(m-\alpha)}{\Gamma(-\alpha)\Gamma(m+1)} = (-1)^m\binom{\alpha}{m},\ m=0,1,\ldots,M.$$

It is readily to verify that

$$\begin{cases} g_0 = 1,\ -g_1 = \alpha > 0,\ g_m \geq g_{m+1} \geq 0,\ m \geq 2; \\ \sum_{m=0}^{M} g_m \leq 0,\ M \in \mathbb{Z}^+;\ \sum_{m=0}^{\infty} g_m = 0. \end{cases} \tag{2.4}$$

Now, let $K \in \mathbb{Z}^+,\ K \gg 1$, and $h = a/(K+1)$. Denoting $x_0 = 0,\ x_{K+1} = a$, we consider the mesh region

$$\Omega_{a,h} = \{x_k, \mid x_k = x_{k-1} + h,\ k = 1,2,\ldots,K\}.$$

On the other hand, we define $T_\tau = \{t_n \mid t_n = \sum_{\ell=1}^{n}\tau_\ell,\ n = 0,1,\ldots,N\}$, where $1 \gg \tau_n > 0$ are variable temporal steps to be determined adaptively, and N is the maximal number of steps to reach. We further denote $u_k = u(x_k,t),\ d_k = d(x_k,t),\ f_k = f(u_k),\ k = 0,1,\ldots,K+1$. A fractional CFL number may be defined as $\mu_\alpha = \tau/h^\alpha$, τ can be the average of temporal steps used [19].

Let u_k be an approximation of the exact solution of (2.1)–(2.3) at $(x_k,t) \in \Omega_{a,h}\times T_{\Delta t}$. It is shown in [16] that

$$\frac{\partial^\alpha u(x_k,t)}{\partial x^\alpha} = \frac{1}{h^\alpha}\left[\left(1-\frac{\alpha}{2}\right)\sum_{j=0}^{k} g_j u_{k-j} + \frac{\alpha}{2}\sum_{j=0}^{k+1} g_j u_{k-j+1}\right] + \mathcal{O}(h^2),\ h\to 0^+. \tag{2.5}$$

It has been proven that (2.5) coincides with the standard second-order central difference approximation of the second derivative when $\alpha = 2$ [18].

An application of (2.5) to (2.1) yields our semi-discretized differential system

$$(u_t)_k = \frac{d_k}{h^\alpha}\left[\left(1-\frac{\alpha}{2}\right)\sum_{j=0}^{k} g_j u_{k-j} + \frac{\alpha}{2}\sum_{j=0}^{k+1} g_j u_{k-j+1}\right] + f_k,\quad k = 1,2,\ldots,K.$$

The above together with conditions (2.2), (2.3) can be conveniently expressed as

$$v_t = Cv + f(v),\ 0 < t < T;\ v(0) = v_0, \tag{2.6}$$

where $v = (u_1,u_2,\ldots,u_K)^\intercal,\ f = (f_1,f_2,\ldots,f_K)^\intercal \in \mathbb{R}^K$ and $C = (c_{ij}) \in \mathbb{R}^{K\times K}$ for which

$$c_{ij} = \begin{cases} \frac{d_i}{h^\alpha}\left[\left(1-\frac{\alpha}{2}\right)g_0 + \frac{\alpha}{2}g_1\right], & i = j, \\ \frac{d_i}{h^\alpha}\left[\left(1-\frac{\alpha}{2}\right)g_{i-j} + \frac{\alpha}{2}g_{i-j+1}\right], & i \leq j, \\ \frac{d_i\alpha g_0}{2h^\alpha}, & j = i+1, \\ 0, & \text{otherwise.} \end{cases}$$

A formal solution of (2.6) takes the form

$$v(t+\tau) = e^{\tau C}v(t) + \int_t^{t+\tau} e^{(t+\tau-\xi)C}f(v(\xi))d\xi,\quad t,\tau \geq 0.$$

A trapezoidal rule for the integral leads to following approximation of the above:

$$v(t+\tau) = e^{\tau C}v(t) + \frac{\tau}{2}\left[f(v(t+\tau)) + e^{\tau C}f(v(t))\right] + \mathcal{O}(\tau^2),\quad t \geq 0,\ \tau\to 0^+. \tag{2.7}$$

The matrix exponential operator can then be handled via an A-stable [1/1] Padé approximant, this is,

$$e^{\tau C} = \left(I - \frac{\tau}{2}C\right)^{-1}\left(I + \frac{\tau}{2}C\right) + \mathcal{O}(\tau^2),\ \tau\to 0^+. \tag{2.8}$$

Thus, from (2.7) and (2.8) we obtain the following fully discretized second-order scheme,

$$v_n = \left(I - \frac{\tau_n}{2}C\right)^{-1}\left(I + \frac{\tau_n}{2}C\right)\left(v_{n-1} + \frac{\tau_n}{2}f_{n-1}\right) + \frac{\tau_n}{2}f_n,\ n = 1,2,\ldots,N, \tag{2.9}$$

$$v_0 = (u_1(0),u_2(0),\ldots,u_K(0))^\intercal. \tag{2.10}$$

where functions $\psi_\ell = \psi(t_\ell),\ t_\ell \in T_\tau$. We may further employ an Euler method for evaluating $f_n \approx f(v_{n-1} + \tau_n(Cv_{n-1} + f_{n-1}))$ in a linearization procedure [4]. Therefore, the overall truncation error of our scheme (2.9), (2.10) should be $\mathcal{O}(h^2 + \tau_n)$. In the situation for maintaining a constant or a near constant CFL number, we would expect the error to be at $\mathcal{O}(h^\alpha)$.

It has been shown that quenching solutions are extremely sensitive over time due to their distinctive singularities [3,4,20]. Similar to semi-adaptive procedures considered in [2,13,21], we adopt following arc-length monitor function of u_t:

$$m(u_t, t) = \max_{0\le x\le a} \sqrt{1 + u_{tt}^2}, \quad t \ge 0.$$

Recall that $\tau_{n+1} = t_{n+1} - t_n,\ n = 1, 2, \ldots, N-1$, are variable temporal steps. They satisfy the following quadratic formulation,

$$\tau_{n+1}^2 = \frac{1 + \max_{0\le x\le a}\left(u_{tt}^{n-1/2}\right)^2}{1 + \max_{0\le x\le a}\left(u_{tt}^{n+1/2}\right)^2}\,\tau_n^2, \quad n = 1, 2, \ldots, N-1. \tag{2.11}$$

Once $\tau_0 > 0$ is chosen, the subsequently adaptive temporal steps can be approximately calculated through (2.11) and under proper smoothness constraints [4,9,12].

3. Analysis of positivity, monotonicity and stability

3.1. Solution positivity and monotonicity

Kawarada problems (1.1)–(1.3) and (2.1)–(2.3) are known for their rich properties related to multi-physics applications especially in fuel combustions and cell biology (see [1,3,4,8] and the references therein for further details). It is anticipated that the sequence of numerical solution, $\{v^n\}_{n=0}^N$, generated by (2.9), (2.10) must be positive and monotonically increasing [2,9,13,15]. Let us define $\mu_{\alpha,n} = \max_n(\tau_n)/h^\alpha$, for $n = 1, 2, \ldots$.

Theorem 3.1. *If $\frac{\sqrt{17}-1}{2} \le \alpha \le 2$, then $I - \frac{\tau_n}{2}C$ is strictly diagonally dominant, monotone and inverse positive.*

Proof. Let $A = I - \frac{\tau_n}{2}C$. We consider its diagonal element

$$a_{kk} = 1 - \frac{\tau_n d_k}{2h^\alpha}\left[\left(1 - \frac{\alpha}{2}\right)g_0 + \frac{\alpha}{2}g_1\right] = 1 + \frac{\tau_n d_k}{2h^\alpha}\left[\frac{\alpha^2}{2} + \frac{\alpha}{2} - 1\right].$$

If $1 < \alpha < 2$, then $\frac{\alpha^2}{2} + \frac{\alpha}{2} - 1 > 0$. Thus, $a_{kk} > 0$. Recall (2.4) and the fact that $1 < \alpha < 2$, we have $\frac{\alpha}{2}g_{k-j+1} + \left(1 - \frac{\alpha}{2}\right)g_{k-j} > 0$ for $k < j - 2$. Further, to ensure $\frac{\alpha}{2}g_2 + \left(1 - \frac{\alpha}{2}\right)g_1 > 0$, similar to that in [16], a sufficient condition must be

$$\frac{\sqrt{17} - 1}{2} \le \alpha \le 2. \tag{3.1}$$

Now, we consider absolute sums of off-diagonal elements of A. To this end,

$$\begin{aligned} r_i &= \sum_{j=1, j\ne i}^{K} |a_{ij}| = \frac{\tau_n d_i}{2h^\alpha}\left\{\sum_{k=1}^{i-1}\left[\frac{\alpha}{2}g_{i-k+1} + \left(1 - \frac{\alpha}{2}\right)g_{i-k}\right] + \frac{\alpha}{2}g_0\right\} \\ &= \frac{\tau_n d_i}{2h^\alpha}\left[\frac{\alpha}{2}\left(g_i + g_{i-1} + \cdots + g_2 + g_0\right) + \left(1 - \frac{\alpha}{2}\right)\left(g_{i-1} + \cdots + g_1\right)\right] \\ &\le \frac{\tau_n d_i}{2h^\alpha}\left[\frac{\alpha}{2} \times (-g_1) + \left(1 - \frac{\alpha}{2}\right) \times (-g_0)\right] \\ &= \frac{\tau_n d_i}{2h^\alpha}\left(\frac{\alpha^2}{2} + \frac{\alpha}{2} - 1\right), \quad i = 1, 2, \ldots, K. \end{aligned}$$

Since

$$r_i = \sum_{j=1, j\ne i}^{K} |a_{ij}| < \frac{\tau_n d_i}{2h^\alpha}\left(\frac{\alpha^2}{2} + \frac{\alpha}{2} - 1\right) + 1 = a_{ii},\ i = 1, 2, \ldots, K,$$

Therefore A is strictly diagonally dominant and thus invertible.

Moreover, based on particular features of A, we have the following properties.

1. $\frac{\alpha}{2}g_0 > 0$, $\left(1-\frac{\alpha}{2}\right)g_{i-1}+\frac{\alpha}{2}g_i > 0$, $i = 1, \ldots, K-1$, since $\left(1-\frac{\alpha}{2}\right)g_0+\frac{\alpha}{2}g_1 = -\left(\frac{\alpha^2}{2}+\frac{\alpha}{2}-1\right) < 0$. In other words, all nonzero diagonal entries of A are positive, while all nontrivial off-diagonal entries of the matrix are negative.
2. We have $\sum_{j=1}^{K} a_{ij} = 1-\frac{\tau_n d_i}{2h^\alpha}\left[\left(1-\frac{\alpha}{2}\right)(g_0+g_1+\cdots+g_{i-1})+\frac{\alpha}{2}(g_i+g_{i-1}+\cdots+g_0)\right]$, $i = 1, 2, \ldots, K-1$. Further, recall (2.4). We have $\sum_{j=0}^{i-1} g_j \le 0$ and $\sum_{j=0}^{i} g_j \le 0$. It follows subsequently that $\sum_{j=1}^{K} a_{ij} > 0$ for $i = 1, 2, \ldots, K-1$. As $i = K$, the same result can be obtained for $\sum_{j=1}^{i} g_j \le -1$.

Thus, A is monotone and inversely positive following the weak-row sum criterion [22]. This completes our proof. □

Theorem 3.2. *If*

$$\mu_{\alpha,n} < \frac{1}{2d_{max}}, \quad \frac{\sqrt{17}-1}{2} \le \alpha \le 2, \tag{3.2}$$

where $d_{max} = \max_{1\le k\le K} d_k$, *then* $I+\frac{\tau_n}{2}C$ *is positive and nonsingular.*

Proof. Let $B = I+\frac{\tau_n}{2}C$. Recall (2.4) and (3.2). Off-diagonal entries of B must be positive. Now, we consider the diagonal elements of B,

$$b_{ii} = 1+\frac{\tau_n d_i}{2h^\alpha}\left[\left(1-\frac{\alpha}{2}\right)g_0+\frac{\alpha}{2}g_1\right] = 1-\frac{\tau_n d_i}{2h^\alpha}\left(\frac{\alpha^2}{2}+\frac{\alpha}{2}-1\right) \ge 1-\frac{\tau_n d_i}{h^\alpha},\ i = 1, 2, \ldots, K.$$

According to (3.2), we must have $\frac{\tau_n d_k}{h^\alpha} < 1$. Therefore $b_{ii} > 0$. Again, recall (2.4) and the fact that $1 < \alpha < 2$, we have $g_{i-j+1}\frac{\alpha}{2}+g_{i-j}\left(1-\frac{\alpha}{2}\right) > 0$ for any $i < j-2 \le K-2$. Now, we observe that $g_2\frac{\alpha}{2}+g_1\left(1-\frac{\alpha}{2}\right) > 0$ because of (3.1). Therefore $a_{ij} > 0$ for $i,\ j = 1, \ldots, K$. This ensures the positivity of B. Then we consider the sup-num of $\frac{\tau_n}{2}C$, *that is,*

$$\begin{aligned}
\left\|\frac{\tau_n}{2}C\right\|_\infty &= \max_i\left\{\frac{\tau_n d_i}{2h^\alpha}\sum_{j=1}^{K}|C_{ij}|\right\}\\
&= \max_i\left\{\frac{\tau_n d_i}{2h^\alpha}\sum_{k=1}^{i-1}\left[\frac{\alpha}{2}g_{i-k+1}+\left(1-\frac{\alpha}{2}\right)g_{i-k}\right]+\frac{\alpha}{2}g_0-\left[\frac{\alpha}{2}g_1+(1-\frac{\alpha}{2})g_0\right]\right\}\\
&\le \frac{\max_n(\tau_n)d_{max}}{h^\alpha}\left(\frac{\alpha^2}{2}+\frac{\alpha}{2}-1\right).
\end{aligned}$$

It is clear that $\frac{\alpha^2}{2}+\frac{\alpha}{2}-2 > 0$ if $\frac{\sqrt{17}-1}{2} \le \alpha \le 2$. Further, if $\mu_{\alpha,n} < 1/(2d_{max})$, then $\frac{\tau_n}{2}\|C\|_\infty < 1$. Therefore B is nonsingular [22]. □

Lemma 3.1. *Let* $v_0 = 0$ *and* $\tau_1 \ge 0$ *be a beginning temporal step. If* (3.2) *holds and* $\tau_1 < \sigma^{-1}$, *where* $\sigma = \max(f(\tau_1 f_0))$, *then* $v_1 > v_0$ *and* $\|v_1\|_\infty < 1$.

Proof. Utilizing (2.9), we find that

$$\begin{aligned}
v_1 &= \left(I-\frac{\tau_1}{2}C\right)^{-1}\left(I+\frac{\tau_1}{2}C\right)\left(v_0+\frac{\tau_1}{2}f_0\right)+\frac{\tau_1}{2}f_1\\
&= \frac{\tau_1}{2}\left[\left(I-\frac{\tau_1}{2}C\right)^{-1}\left(I+\frac{\tau_1}{2}C\right)f_0+f(\tau_1 f_0)\right].
\end{aligned}$$

Thus, $v_1 > v_0 = 0$ due to Theorems 3.1 and 3.2. We next show that $\|v_1\|_\infty < 1$. To this end, we define $X = (1, 1, \ldots, 1)^\intercal$ and consider the difference

$$v_1 - X = \left(I-\frac{\tau_1}{2}C\right)^{-1}\left[\frac{\tau_1}{2}\left(I+\frac{\tau_1}{2}C\right)f_0+\frac{\tau_1}{2}\left(I-\frac{\tau_1}{2}C\right)f(\tau_1 f_0)-\left(I-\frac{\tau_1}{2}C\right)X\right].$$

Now, define

$$\begin{aligned}
W_1 &= \frac{\tau_1}{2}\left(I+\frac{\tau_1}{2}C\right)f_0+\frac{\tau_1}{2}\left(I-\frac{\tau_1}{2}C\right)f(\tau_1 f_0),\ W_2 = -\left(I-\frac{\tau_1}{2}C\right)X,\\
W &= W_1+W_2.
\end{aligned}$$

In this case $v_1 - X = \left(I-\frac{\tau_1}{2}C\right)^{-1}W$. Since (3.2) holds, the matrix $I-\frac{\tau_1}{2}C$ is inverse positive. In addition

$$\begin{aligned}
W_1 &= \frac{\tau_1}{2}\left(I+\frac{\tau_1}{2}C\right)f_0+\frac{\tau_1}{2}\left(I-\frac{\tau_1}{2}C\right)f(\tau_1 f_0)\\
&\le \frac{\tau_1}{2}\left[\left(I+\frac{\tau_1}{2}C\right)+\left(I-\frac{\tau_1}{2}C\right)\right]f(\tau_1 f_0) = \tau_1 f(\tau_1 f_0).
\end{aligned} \tag{3.3}$$

Because $\sum_{j=0}^{i} g_j \le \sum_{j=0}^{\infty} g_j = 0$ due to (2.4), we have $CX \le 0$. Hence

$$W_2 = -X + \frac{\tau_1}{2} CX \le -X.$$

Combining the above with (3.3), we acquire that $W \le \tau_1 f(\tau_1 f_0) - X < \tau_1 \max(f(\tau_1 f_0)) - 1 = \tau_1 \sigma - 1$. If $\tau_1 < \sigma^{-1}$, we have $W < 0$ which completes our proof. □

Lemma 3.2. *If (3.2) holds for any temporal step τ_n that is sufficiently small, and $0 \le v_{n-1} < 1$ such that $Cv_{n-1} + f_{n-1} > 0$ then solution vectors of (2.9), $\{v_n\}_{n=0}^{\infty}$,*

1. *form a monotonically increasing sequence and*
2. *have $Cv_n + f_n > 0$, $n \ge 0$.*

Proof. First, based on Lemma 3.1, we may claim that $v_1 > v_0$. We then let f_n in (2.9) be approximated through an Euler formula, *that is,* $f_n = f_{n-1} + \tau_n M(Cv_{n-1} + f_{n-1}) + \mathcal{O}(\tau_n^2)$, $n \ge 1$, Recalling (2.9), we observe that

$$\begin{aligned} v_n - v_{n-1} &= \left(I - \frac{\tau_n}{2}C\right)^{-1} \left[\left(I + \frac{\tau_n}{2}C\right)\left(v_{n-1} + \frac{\tau_n}{2} f_{n-1}\right) \right. \\ &\quad \left. + \frac{\tau_n}{2}\left(I - \frac{\tau_n}{2}C\right) f_n - \left(I - \frac{\tau_n}{2}C\right) v_{n-1}\right] \\ &= \left(I - \frac{\tau_n}{2}C\right)^{-1} \left[\tau_n C v_{n-1} + \frac{\tau_n}{2} f_{n-1} + \frac{\tau_n}{2} f_n + \frac{\tau_n^2}{4} C(f_{n-1} - f_n)\right] \\ &\ge \tau_n \left(I - \frac{\tau_n}{2}C\right)^{-1} \left[C v_{n-1} + f_{n-1} - \frac{\tau_n}{4} C(f_n - f_{n-1})\right], \ n > 1, \end{aligned}$$

due to the property $f_n > f_{n-1}$. Based on Taylor's theorem [23], for $n > 1$,

$$v_n - v_{n-1} \ge \tau_n \left(I - \frac{\tau_n}{2}C\right)^{-1} \left[(Cv_{n-1} + f_{n-1}) - \frac{M\tau_n^2}{4} C(Cv_{n-1} + f_{n-1})\right], \tag{3.4}$$

where M is the positive diagonal Jacobian matrix of $f(v)$ evaluated at some mean value point. Thus, $v_n > v_{n-1}$ if τ_n is sufficiently small.

On the other hand, it is evident that

$$\begin{aligned} Cv_n + f_n &= f_n - f_{n-1} + Cv_{n-1} + f_{n-1} + C(v_n - v_{n-1}) \\ &= f_n - f_{n-1} + Cv_{n-1} + f_{n-1} \\ &\quad + C\left[\left(I - \frac{\tau_n}{2}C\right)^{-1}\left(I + \frac{\tau_n}{2}C\right)\left(v_{n-1} + \frac{\tau_n}{2} f_{n-1}\right) + \frac{\tau_n}{2} f_n - v_{n-1}\right] \\ &= f_n - f_{n-1} + \left(I - \frac{\tau_n}{2}C\right)^{-1} \left[\left(I - \frac{\tau_n}{2}C\right)(Cv_{n-1} + f_{n-1}) \right. \\ &\quad \left. + C\left(I + \frac{\tau_n}{2}C\right)\left(v_{n-1} + \frac{\tau_n}{2} f_{n-1}\right) + \left(I - \frac{\tau_n}{2}C\right) C\left(\frac{\tau_n}{2} f_n - v_{n-1}\right)\right] \\ &= f_n - f_{n-1} + \left(I - \frac{\tau_n}{2}C\right)^{-1} \left[\left(I - \frac{\tau_n}{2}C\right)(Cv_{n-1} + f_{n-1}) \right. \\ &\quad \left. + \tau_n C^2 v_{n-1} + \frac{\tau_n}{2} C(f_{n-1} + f_n) + \frac{\tau_n^2}{4} C^2(f_{n-1} - f_n)\right] \\ &\ge f_n - f_{n-1} + \left(I - \frac{\tau_n}{2}C\right)^{-1} \left[\left(I - \frac{\tau_n}{2}C\right)(Cv_{n-1} + f_{n-1}) \right. \\ &\quad \left. + \tau_n C(Cv_{n-1} + f_{n-1}) + \frac{\tau_n^2}{4} C^2(f_{n-1} - f_n)\right] \ = \ f_n - f_{n-1} \\ &\quad + \left(I - \frac{\tau_n}{2}C\right)^{-1} \left[\left(I + \frac{\tau_n}{2}C\right)(Cv_{n-1} + f_{n-1}) + \frac{\tau_n^2}{4} C^2(f_{n-1} - f_n)\right]. \end{aligned}$$

Since $f_n \approx f(v_{n-1} + \tau_n(Cv_{n-1} + f_{n-1}))$ and $f_n > f_{n-1}$. Using Taylor's theorem, we arrive at

$$\begin{aligned} Cv_n + f_n &\ge f_n - f_{n-1} + \left(I - \frac{\tau_n}{2}C\right)^{-1}\left(I - \frac{\tau_n}{2}C\right)\left(I + \tau_n C - \frac{M\tau_n^3}{4}C^2\right) \\ &\quad \times (Cv_{n-1} + f_{n-1}) \\ &= f_n - f_{n-1} + \left(I + \tau_n C - \frac{M\tau_n^3}{4}C^2\right)(Cv_{n-1} + f_{n-1}). \end{aligned}$$

Thus, for sufficiently small τ_n, the matrix $I + \tau_n C - \frac{M\tau_n^3}{4}C^2$ must be positive, where M is defined as Eq. (3.4). Therefore our lemma is true. □

As consequences of the two lemmas, we may state the following two theorems for the monotonic growth and linear stability properties of the numerical solution generated by (2.9), (2.10).

Theorem 3.3. *If (3.2) holds for all $n \geq \ell \geq 0$ and $v_0 \geq 0$, such that $Cv_0 + f_0 > 0$, then the sequence $\{v_n\}_{n\geq\ell}$ produced by the semi-adaptive scheme (2.9), (2.10) increases monotonically.*

Proof. The theorem is a straightforward consequence from Lemmas 3.1 and 3.2. □

3.2. Numerical stability

Stability has been an extremely difficult issue while solving nonlinear quenching-type problems such as (1.1)–(1.3) and (2.1)–(2.3). However, if the solution is varying relatively slowly, instability may be detected through conventional linear stability analysis of the algorithms involved [20,24,25]. Though such a consideration cannot be rigorously justified, the information obtained has been found to be practically meaningful and important [2,8,15]. We continue analyzing the stability of the finite difference scheme (2.9), (2.10), for which the nonlinear term is frozen, in this section. To freeze a nonlinear term is a typical linearization process in which the unknown function is replaced by a known quantity. This eliminates the nonlinearity temporarily so that a conventional linear stability analysis can be carried out. Although a linear stability can never be justified for replacing a nonlinear stability in the global sense, it may reflect effectively the local solvability when temporal mesh step sizes used are sufficiently small [2,26].

Definition 3.1 (*[23,27]*)**.** Let $N > 0$ be sufficiently large. Further, let $v_k^n,\ \tilde{v}_k^n,\ 1 \leq k \leq K,\ 0 \leq n \leq N$, be the true and perturbed solutions of a finite difference scheme, respectively. Denote $\epsilon^n = (\epsilon_1^n, \epsilon_2^n, \ldots, \epsilon_K^n)^\intercal$, where $\epsilon_k^n = v_k^n - \tilde{v}_k^n,\ 1 \leq k \leq K$. We say that the scheme is numerically stable if $\|\epsilon^n\| \leq \|\epsilon^0\|,\ 0 \leq n \leq N$, holds for any suitable Euclidean norm.

Theorem 3.4. *If (3.2) holds for all $n \geq \ell \geq 0$, then the semi-adaptive scheme (2.9), (2.10) is conditionally numerically stable when f is frozen.*

Proof. Let $v_k^n,\ \tilde{v}_k^n,\ 1 \leq k \leq K,\ 0 \leq n \leq N$, be the true and perturbed solutions of (2.9), (2.10), respectively. Denote $\zeta_k^n = \frac{\tau_n d_k}{2h^\alpha},\ \epsilon_k^n = v_k^n - \tilde{v}_k^n,\ 1 \leq k \leq K$, and set $\epsilon^n = (\epsilon_1^n, \epsilon_2^n, \ldots, \epsilon_K^n)^\intercal,\ 0 \leq n \leq N$. We show the theorem through a mathematical induction. To this end, we first notice that, when f is frozen,

$$\left(I - \frac{\tau_n}{2}C\right)\epsilon^{n+1} = \left(I + \frac{\tau_n}{2}C\right)\epsilon^n, \quad n = 0, 1, \ldots, N-1,$$

where C is defined in (2.6). Secondly, recall (3.2). We find that

$$\left(1 - \frac{\alpha}{2}\right)g_0 + \frac{\alpha}{2}g_1 < 0, \quad \left(1 - \frac{\alpha}{2}\right)g_{k-1} + \frac{\alpha}{2}g_k > 0, \quad k = 2, 3, \ldots, K;$$
$$1 + \zeta_k^n\left(1 - \frac{\alpha}{2}\right)g_0 + \zeta_k^n\frac{\alpha}{2}g_1 > 0, \quad k = 1, 2, \ldots, K,\ n = 0, 1, \ldots, N.$$

For $n = 1$, recalling (2.4) we must have

$$\begin{aligned}
\left\|\epsilon^1\right\|_\infty &= \max_{1\leq j\leq K}\left|\epsilon_j^1\right| = \left|\epsilon_1^1\right| \leq \left|\epsilon_\ell^1\right| - \zeta_\ell^1\left(1 - \frac{\alpha}{2}\right)\sum_{k=0}^{\ell-1} g_k\left|\epsilon_\ell^1\right| - \zeta_\ell^1\frac{\alpha}{2}\sum_{k=0}^{\ell} g_k\left|\epsilon_\ell^1\right| \\
&\leq \left[1 - \zeta_\ell^1\left(1 - \frac{\alpha}{2}\right)g_0 - \zeta_\ell^1\frac{\alpha}{2}g_1\right]\left|\epsilon_l^1\right| - \zeta_\ell^1\frac{\alpha}{2}g_0\left|\epsilon_{\ell+1}^1\right| \\
&\quad - \zeta_\ell^1\sum_{k=2}^{\ell}\left[\left(1 - \frac{\alpha}{2}\right)g_{k-1} + \frac{\alpha}{2}g_k\right]\left|\epsilon_{\ell-k+1}^1\right| \\
&= \left[1 + \zeta_\ell^0\left(1 - \frac{\alpha}{2}\right)g_0 + \zeta_\ell^0\frac{\alpha}{2}g_1\right]\left|\epsilon_\ell^0\right| \\
&\quad + \zeta_\ell^0\frac{\alpha}{2}g_0\left|\epsilon_{\ell+1}^0\right| + \zeta_\ell^0\sum_{k=2}^{\ell}\left[\left(1 - \frac{\alpha}{2}\right)g_{k-1} + \frac{\alpha}{2}g_k\right]\left|\epsilon_{\ell-k+1}^0\right| \\
&\leq \left[1 + \zeta_\ell^0\left(1 - \frac{\alpha}{2}\right)\sum_{k=0}^{\ell-1} g_k + \zeta_\ell^0\frac{\alpha}{2}\sum_{k=0}^{\ell} g_k\right]\max_{1\leq j\leq K}\left|\epsilon_j^0\right| \\
&\leq \max_{1\leq j\leq K}\left|\epsilon_j^0\right| = \left\|\epsilon^0\right\|_\infty.
\end{aligned}$$

Note that $\|\epsilon^1\|_\infty = |\epsilon_K^1|$ due to the fact that $\sum_{k=1}^K g_k \le -1$. Consequently, we acquire from the above that

$$\begin{aligned}
\|\epsilon^1\|_\infty &= |\epsilon_K^1| \le |\epsilon_K^1| - \zeta_K^1\left(1-\frac{\alpha}{2}\right)\sum_{k=0}^{K-1} g_k |\epsilon_K^1| - \zeta_K^1\frac{\alpha}{2}\sum_{k=1}^{K} g_k |\epsilon_K^1| \\
&\le \left[1-\zeta_K^1\left(1-\frac{\alpha}{2}\right)g_0 - \zeta_K^1\frac{\alpha}{2}g_1\right]|\epsilon_K^1| - \zeta_K^1\sum_{k=2}^{K}\left[\left(1-\frac{\alpha}{2}\right)g_{k-1}+\frac{\alpha}{2}g_k\right]|\epsilon_{K-k+1}^1| \\
&= \left[1+\zeta_K^0\left(1-\frac{\alpha}{2}\right)g_0 + \zeta_K^0\frac{\alpha}{2}g_1\right]|\epsilon_K^0| + \zeta_K^0\sum_{k=2}^{K}\left[\left(1-\frac{\alpha}{2}\right)g_{k-1}+\frac{\alpha}{2}g_k\right]|\epsilon_{k-K+1}^0| \\
&\le \left[1+\zeta_K^0\left(1-\frac{\alpha}{2}\right)\sum_{k=0}^{K-1} g_k + \zeta_K^0\frac{\alpha}{2}\sum_{k=1}^{K} g_k\right]\max_{1\le j\le K}|\epsilon_j^0| \\
&\le \max_{1\le j\le K}|\epsilon_j^0| = \|\epsilon^0\|_\infty . \qquad (3.5)
\end{aligned}$$

Suppose that $\|\epsilon^j\|_\infty \le \|\epsilon^0\|_\infty$ for $j = 1, 2, \ldots, n-1$. Again, recall (2.4). For $\frac{\sqrt{17}-1}{2} \le \alpha \le 2$, we observe that

$$\begin{aligned}
\|\epsilon^n\|_\infty &= \max_{1\le j\le K}|\epsilon_j^n| = |\epsilon_\ell^n| \le |\epsilon_\ell^n| - \zeta_\ell^n\left(1-\frac{\alpha}{2}\right)\sum_{k=0}^{\ell-1} g_k |\epsilon_\ell^n| - \zeta_\ell^n\frac{\alpha}{2}\sum_{k=0}^{\ell} g_k |\epsilon_\ell^n| \\
&\le \left[1-\zeta_\ell^n\left(1-\frac{\alpha}{2}\right)g_0 - \zeta_\ell^n\frac{\alpha}{2}g_1\right]|\epsilon_\ell^n| - \zeta_\ell^n\frac{\alpha}{2}g_0|\epsilon_{\ell+1}^n| \\
&\quad - \zeta_\ell^n\sum_{k=2}^{\ell}\left[\left(1-\frac{\alpha}{2}\right)g_{k-1}+\frac{\alpha}{2}g_k\right]|\epsilon_{\ell-k+1}^n| \\
&= \left[1+\zeta_\ell^{n-1}\left(1-\frac{\alpha}{2}\right)g_0 + \zeta_\ell^{n-1}\frac{\alpha}{2}g_1\right]|\epsilon_\ell^{n-1}| \\
&\quad + \zeta_\ell^{n-1}\frac{\alpha}{2}g_0|\epsilon_{\ell+1}^{n-1}| + \zeta_\ell^{n-1}\sum_{k=2}^{\ell}\left[\left(1-\frac{\alpha}{2}\right)g_{k-1}+\frac{\alpha}{2}g_k\right]|\epsilon_{\ell-k+1}^{n-1}| \\
&\le \left[1+\zeta_\ell^{n-1}\frac{\alpha}{2}\sum_{k=0}^{\ell} g_k + \zeta_n^{n-1}\left(1-\frac{\alpha}{2}\right)\sum_{k=0}^{\ell-1} g_k\right]\max_{1\le j\le K}|\epsilon_j^{n-1}| \\
&\le \max_{1\le j\le K}|\epsilon_j^{n-1}| = \|\epsilon^{n-1}\|_\infty . \qquad (3.6)
\end{aligned}$$

Based on our hypothesis, it is immediately clear that $\|\epsilon^j\|_\infty \le \|\epsilon^0\|_\infty$ for $j = 1, 2, \ldots, N$. By the same token, we have $\|\epsilon^n\|_\infty = |\epsilon_K^n|$. Since situations for (3.5) and (3.6) are similar, the proof of the theorem is thus completed. □

4. Simulation experiments

We consider a sequence of computational experiments in the section to validate and illustrate anticipated critical domains, quenching times, and quenching locations of the fractional Kawarada problem (2.1)–(2.3) without a degeneracy, *that is,* $d(x,t) \equiv 1$.

To examine aforementioned key mathematical features of the solution and our algorithm (2.9), (2.10), we first set $\alpha = 2$. Thus, we may compare our numerical solution directly to known results related to the conventional integer order Kawarada problem (1.1)–(1.3). Our semi-adaptation only kicks in during final stages of computations, say, as

$$\delta \le \max_{0\le x\le a} u(x,t) < 1,$$

where $\delta > 0$ is chosen to be close to one, for maximizing the computational efficiency.

Case I: $\alpha = 2$

Set $F(x) \equiv 0$. While it is known in the case that the critical length $a^\star \approx 1.5303$ [1,5,6,10], our computations indicate that $a^\star \approx 1.53125$, which is consistent with the existing result.

Based on the above, we conduct a study of corresponding quenching times T_a for $a = 1.55,\ 2,\ \pi$ and 10. Initial temporal step $\tau_1 = (1/2)\times 10^{-4}$ and spatial step $h = a\times 10^{-2}$ are used. An initial CFL number $\lambda_1 = 1/(2a^2)$ is utilized [23]. Our results are shown in Table 1 together with those obtained by Chan and Chen for $a = \pi$, $0.5 \le T_a \le 0.6772$ [6] and Mooney and Sheng et al. [13,20,25] for $a = 1.55,\ 2$. Standard Crank–Nicolson scheme and Newton iterations are used in the former and compounded adaptive finite difference algorithms are developed in the latter. Let T_a^M be the quenching time given by [20,25] and T_a^S be the quenching time given by [13]. It is found that our results are well consistent with

Table 1
Correlations between the quenching time T_a and domain size a, as compared with T_a^M given by [20,25] and T_a^S by [13].

a	T_a	T_a^M	T_a^S
1.55	3.966	3.963	3.961
2	0.7798	0.779	0.779
π	0.5382	0.538	0.537
10	0.5004	0.5	0.5

Table 2
Monotone convergence of T_a as $a \to \infty$ (T_a^S values are from [4,13]).

a	T_a	T_a^S	a	T_a	T_a^S	a	T_a	T_a^S	a	T_a	T_a^S
1.55	3.966	3.961	1.80	0.9996	0.999	3.00	0.5472	0.546	5.00	0.5026	0.503
1.60	2.0103	2.007	1.90	0.8642	0.871	π	0.5382	0.537	10.00	0.5004	0.500
1.70	1.2572	1.257	2.00	0.7798	0.779	4.00	0.511	0.511	50.00	0.5004	0.500

Table 3
Numerical solution $u(a/2, t)$ and theoretical estimates $u_F(a/2, t)$ offered by (4.1) ($a = 2$, $h = a \times 10^{-2}$, $\tau = 0.5 \times 10^{-4}$ and $F(x) \equiv 0$).

t	u(a/2,t)	$u_F(a/2, t)$	t	u(a/2,t)	$u_F(a/2, t)$
0.7772	0.94261	0.9279	0.7774	0.94491	0.9307
0.7776	0.94732	0.9337	0.7778	0.94986	0.9368
0.7780	0.95254	0.9400	0.7782	0.95539	0.9434
0.7784	0.95845	0.9471	0.7786	0.96176	0.9510
0.7788	0.96539	0.9553	0.7790	0.96944	0.9600
0.7792	0.97408	0.9654	0.7794	0.97962	0.9717
0.7796	0.98677	0.9800	–	–	–

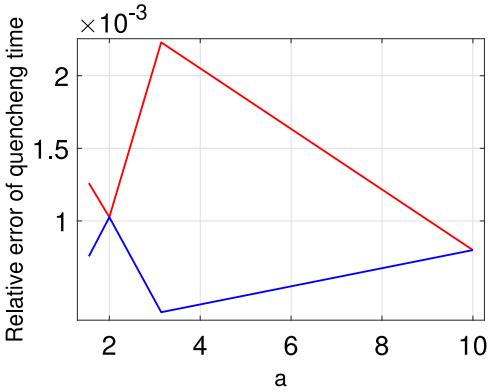

Fig. 1. Relative errors of T_a *vs.* a when $\alpha = 2$. Computations are based on algorithms utilizing (2.9), (2.10). Red curve is for calculations together with an adaptation suggested by [13]. Blue curve is for those when an adjustment introduced by [20,25] is considered. (For interpretation of the references to color in this figure legend, the reader is referred to the web version of this article.)

existing predictions T_a^M and T_a^S. Relative errors of our quenching time T_a with respect to T_a^M and T_a^S are given in Fig. 1. It can be observed that the computed errors are acceptable within the range of numerical accuracy.

Table 2 is devoted to a demonstration of the monotone decay of T_a to 1/2 as the interval size a increases. We have compared our results with those obtained by Sheng, Khaliq and Ge [4,13,21] in Fig. 2, and again the results are satisfactory.

It is worthwhile to mention that, for $a = 2$, Filippas and Guo observe that all quenching solutions of (2.1)–(2.3) with $F \equiv 0$ satisfy the following theoretical expectation [3]:

$$\lim_{t \to T_a} u(1, t) = 1 - \sqrt{2}(T_a - t)^{1/2}. \tag{4.1}$$

In Table 3, numerical solutions are presented together with evaluations based on (4.1) for fixed $a = 2$, $x = 1$ in our final 12 t-steps immediately before quenching. In addition, we give the curve of the relative error between these two results in Fig. 2. It is interesting to see that our numerical solutions precisely reveal this property highlighted by (4.1).

Further, for $a = 2$ and $F(x) = 0.1 \sin \frac{\pi x}{2}$, profiles of the numerical solutions, u and u_t, obtained via (2.9), (2.10) are plotted in Fig. 3 immediately before $T_a^* \approx 0.6964$. Spatially symmetrical profiles of the functions are clearly visible. It can also be seen that the maxima increase monotonically as the time t increases until the unity is reached by u. In fact,

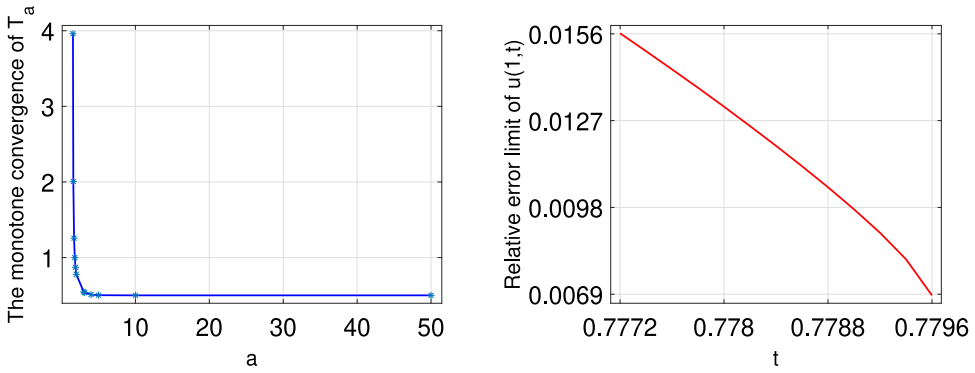

Fig. 2. LEFT: Monotone convergence of T_a as $a \to \infty$. The blue curve is for the quenching time profile obtained in our experiments. Values marked with $\star$ are particular quenching times observed in [13]. An excellent agreement between the both is found; RIGHT: Relative difference between $u(a/2, t)$ and theoretical estimates given by (4.1) ($a = 2,\ h = a \times 10^{-2},\ \tau = 0.5 \times 10^{-4}$ and $F(x) \equiv 0$). (For interpretation of the references to color in this figure legend, the reader is referred to the web version of this article.)

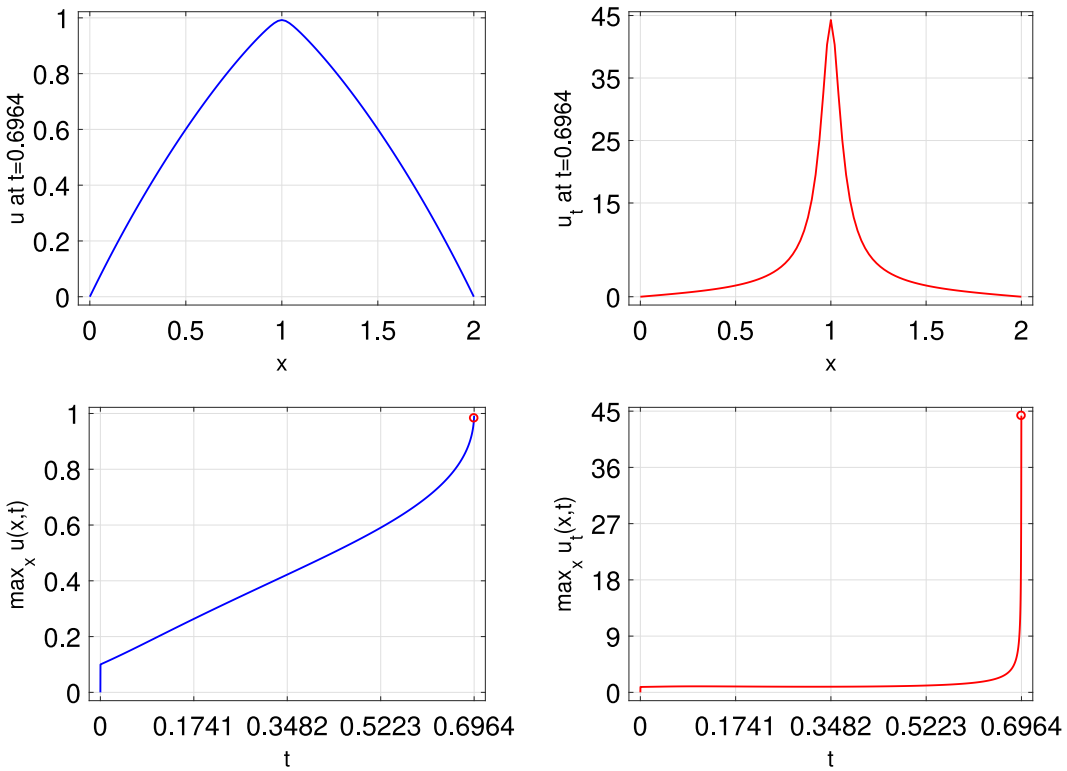

Fig. 3. TOP: profiles of u and u_t immediately before quenching; BOTTOM: profiles of $\max_{0\le x\le a} u$ and $\max_{0\le x\le a} u_t$ *vs.* the time t. Quenching is observed at $T_a^* \approx 0.6964$ for $a = 2$.

a quenching-blow up of the solutions is confirmed by $\max_{0\le x\le 2} u(x, T_2^*) = u(1, T_2^*) \approx 0.99226683$ in our experiments. To see more, in Table 4, we show values of $u,\ u_t$ at different locations. The spatial symmetry of functions is clearly observable. This is consistent with the theoretical expectation [4,10]. For showing more details of the solution structures, we plot three-dimensional surfaces of u and u_t in their final 20 temporal levels priori to quenching in Fig. 4. It is again observable that while u approaches the unity in the center of the spatial domain quickly but peacefully, the derivative u_t rashes to its peak at an altitude of approximately 44.28126959 in a fast and rather violent way as the quenching time T_a^* is approached.

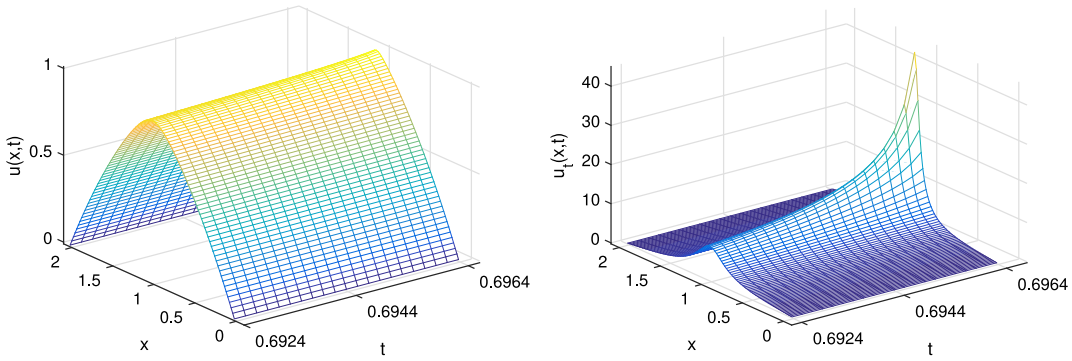

Fig. 4. Three-dimensional views of u and u_t in their final 20 temporal steps immediately before quenching ($0.6924 \le t \le 0.6964$) for $a = 2$. The peak of $u_t(a/2, t)$ is approximately 44.28126959. A quenching phenomenon is observed.

Table 4
Values of functions $u(x, T_a^*)$ and $u_t(x, T_a^*)$ when $a = 2$.

x	0.94	0.96	0.98	1.00	1.02	1.04	1.06
$u(x, T_a^*)$	0.97012708	0.980947412	0.98906719	0.99226683	0.98906722	0.98094746	0.97012713
$u_t(x, T_a^*)$	25.07309149	32.41091340	40.33291633	44.28126959	40.33294449	32.41094593	25.07311756

Table 5
Possible correlations between critical domain sizes and the fractional order α.

α	2	1.95	1.9	1.85	1.80	1.75	1.7	1.65	1.6
a^*	1.53125	1.48437	1.43755	1.39076	1.34398	1.29718	1.25038	1.20355	1.15666

To summarize, our simulation results for the space fractional Kawarada problem (2.1)–(2.3) are satisfactorily consistent to known results of the conventional Kawarada problem as $\alpha = 2$ [6,10,13,20,25]. Thus the new algorithm (2.9), (2.10) is effective and reliable.

Case II: $\alpha \in \left[(\sqrt{17} - 1)/2, 2\right]$

In the circumstance we take $\alpha = 1.8,\ a = 2,\ F(x) = 0.1 \sin \frac{\pi x}{2}$. Typical quenching phenomena are again noticed in our experiments. We show profiles of the numerical solutions $u,\ u_t$ in Fig. 5 up to a quenching time $T^* \approx 0.5946$. Further, profiles of $\max_{0\le x\le a} u$ and $\max_{0\le x\le a} u_t$ immediately before quenching are provided in Fig. 5. The quenching location observed is approximately at $x^* = 0.86$ which is not at the center of spatial interval. We have $u(x^*, T^*) = 0.99945319$. To illustrate more precisely quenching characteristics of the solutions, we plot three-dimensional surfaces of both u and u_t in Fig. 6 for the final 20 temporal steps immediately before quenching. It is found that, while $\max_{0\le x\le a} u$ approaches the unity smoothly, u_t reaches out for a computational peak at about 63.01566851 as $t \to T_a^* \approx 0.5946$.

It has been observed throughout our investigations with various fractional α values, quenching phenomena do occur. However, numerical solutions $u,\ u_t$ do not seem to be symmetric in space as $t \to T_a^*$. Furthermore, locations of $\max_{0\le x\le a} u(x, t),\ \max_{0\le x\le a} u_t(x, t)$ do not in general appear to be at the center of the spatial domain used. Thus it is extremely meaningful to utilize reliable numerical tools for exploring fractional quenching-combustion model problems such as (2.1)–(2.3).

Now, set $F(x) \equiv 0$. For different fractional α values, Table 5 gives different critical domains discovered from our intensive computational experiments. Through the simple computation, we have noticed that the critical interval size decreases to some fixed value between 0.0468 and 0.0470 while the fractional derivative order α decreases from 2 to $\frac{\sqrt{17}-1}{2}$. The discovery is new to the literature and demands further careful investigations. It is interesting to observe that Fig. 7 (left frame) may suggest a linear correlation between the critical domain size and fractional order α as $(\sqrt{17} - 1)/2 \le \alpha \le 2$.

Table 6 is designed for quenching times with respect to different α values based on distinctive interval domain sizes. Apparently, as α decreases, T_a^* decays monotonically. In Fig. 7 (right frame), relationships between the quenching time T_a^* and α are listed with different lengths a. It is noticed that, when $a \ge 2$, quenching time changes only slightly as the fractional derivative order α increases from $(\sqrt{17} - 1)/2$ to 2. However, for $a < 2$, the corresponding quenching time changes rapidly as the order increases.

In Table 7, Quenching locations x_a with respect to different interval sizes a for $\alpha \in \left[(\sqrt{17} - 1)/2, 2\right]$ are given. In Fig. 8 (left), correlation curves between $x_\alpha - a/2$ and α are given for $a = 1.55, 2, \pi$. We also observe that for a moving from 1.55 to π, terminal local extreme value locations of u shift slowly from right to left across the midpoint of spatial

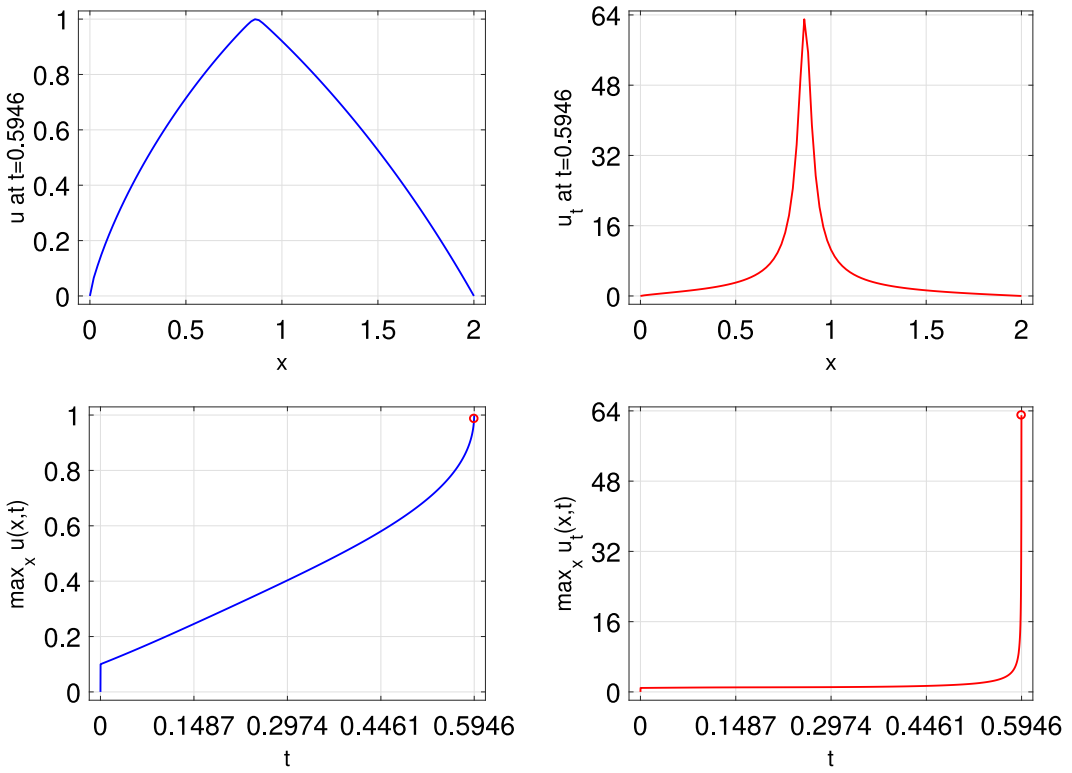

Fig. 5. TOP: u and u_t immediately before quenching. BOTTOM: $\max_x u$ and $\max_x u_t$ vs. t ($\alpha = 1.8,\ a = 2,\ T_2^* \approx 0.5946$).

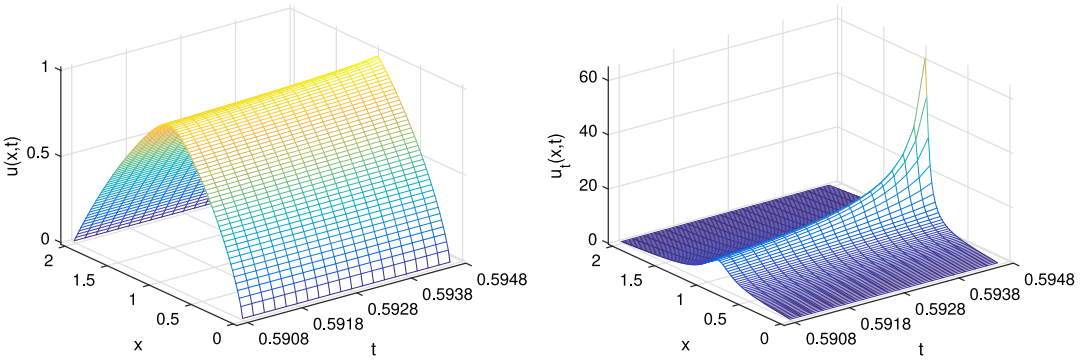

Fig. 6. Three-dimensional views of functions u and u_t in the final 20 temporal steps immediately before quenching ($0.5908 \le t \le 0.5946$). $a = 2$ is used. The peak u_t value is approximately 63.01566851. Quenching is observed.

Table 6
Quenching times T_a^* with respect to different α.

α	2.0	1.95	1.90	1.85	1.80	1.75	1.70	1.65	1.60
$T^\star_{1.55}$	3.966	2.0544	1.5364	1.2716	1.104	0.9856	0.8956	0.8236	0.7644
$T_2^\star$	0.7798	0.7494	0.7224	0.6978	0.6752	0.6546	0.6354	0.6174	0.6008
$T_\pi^\star$	0.5382	0.5368	0.5352	0.5334	0.5316	0.5294	0.5274	0.5252	0.5230
$T^\star_{10}$	0.5004	0.5006	0.5008	0.5008	0.501	0.5012	0.5012	0.5014	0.5014

intervals as α decreasing gradually. Similarly, in the second frame of Fig. 8, curves corresponding to $a = 4, 5, 8, 10, 50$ are given. Terminal local extreme value locations of u shift slowly from left to right across the midpoint of spatial intervals as α decays.

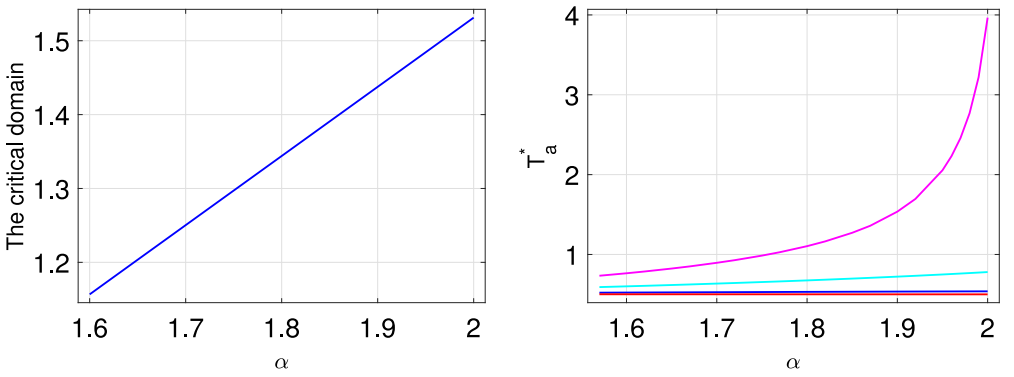

Fig. 7. LEFT: Critical sizes vs. α; RIGHT: Quenching times vs. α. From bottom to top, curves are for $a = 10, \pi, 2, 1.55$, respectively.

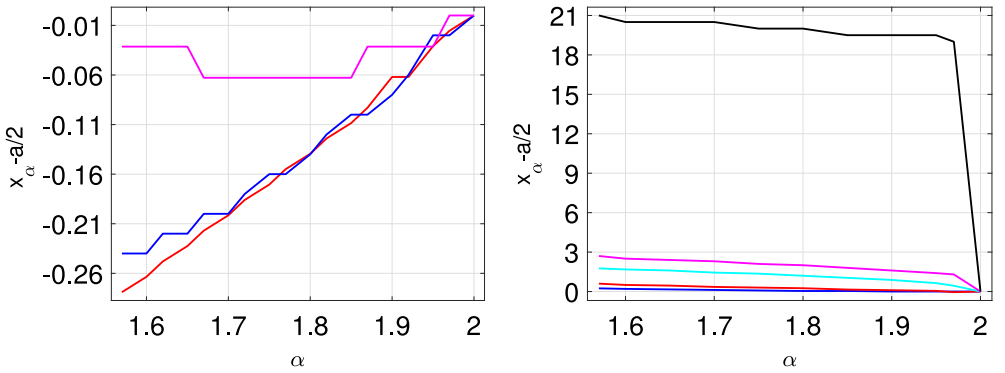

Fig. 8. Correlations between $x_\alpha - a/2$ and α (LEFT: $a = 1.55,\ 2$ and π; RIGHT: $a = 4,\ 5,\ 8,\ 10$ and 50, from the bottom to top respectively).

Table 7
Quenching locations x_α with respect to different interval size a for $(\sqrt{17}-1)/2 \le \alpha \le 2$.

x_α	a							
	1.55	2	π	4	5	8	10	50
$x_{2.0}$	0.775	1	1.5707963	2.0	2.5	4	5	25
$x_{1.95}$	0.7439998	0.98	1.53938395	2.0	2.55	4.64	6.4	44.5
$x_{1.9}$	0.7129998	0.92	1.53938395	2.0	2.6	4.88	6.6	44.5
$x_{1.85}$	0.66649979	0.9	1.50796795	2.04	2.65	5.04	6.8	44.5
$x_{1.8}$	0.63549998	0.86	1.50796795	2.04	2.75	5.2	7.0	45
$x_{1.75}$	0.60449998	0.84	1.50796795	2.08	2.8	5.36	7.10	45
$x_{1.7}$	0.57349998	0.8	1.53938395	2.12	2.85	5.44	7.3	45.5
$x_{1.65}$	0.54249998	0.78	1.53938394	2.16	2.95	5.6	7.4	45.5
$x_{1.6}$	0.51149998	0.76	1.53938395	2.2	3.0	5.68	7.5	45.5

Most parts of our computations are carried out on a MatLab® platform and its parallel computing toolbox on an HP® C3000BL HPC cluster running CentOS® V at Baylor University. The processor consists of 128 nodes, each with 32GB of RAM and dual quad-core Intel 2.6 GHz processors giving a total of 1024 cores. An Infiniband ConnectX® DDR network is used for message passing and networked storage. Shared storage capacity in the cluster is 123TB.

5. Conclusions and forthcoming studies

An effective numerical approach is proposed and analyzed for solving the one-dimensional space-fractional Kawarada problem in this paper. An one-sided Riemann–Liouville fractional Laplacian is employed. The modeling problem exhibits strong quenching singularities but provides a broad spectrum in modern applications.

An optimal α-order finite difference scheme is accomplished for computing the anticipated quenching solutions of the underlying fractional differential equation. In this novel new approach, the fractional derivative is approximated via standard and shifted Grünwald formula combinations. The resulted semi-discretized differential system is then handled through acceptable fractional approximations. Arc-length adaptation is adopted to ensure additional accuracy and reliability throughout the numerical procedure. Criteria to ensure the solution positivity, monotonicity, convergence

and stability are obtained. It is proven that the semi-adaptive algorithm is conditionally stable in the L_∞ conservation sense.

Two sequences of simulation experiments are designed and carried out to validate and confirm that numerical solutions obtained. It is found that results acquired are well consistent with known results and theoretical predictions. In the numerical investigation, fractional order $\alpha = 2$ is firstly selected. Computed solutions are compared with existing integer order quenching problem results published. Secondly, for fractional order $\alpha \in \left[\frac{\sqrt{17}-1}{2}, 2\right]$, computer simulations are conducted to examine key characteristics, features and properties of the fractional quenching problem. New evidences are revealed for fractional quenching solutions including possible correlations between the quenching time and fractional order α, and between quenching locations and α. It is found that the local maximal value point of u shifts from the right to the left across the midpoint of the interval if $a \in (1, \pi]$; and shifts from the left to the right across the midpoint of the interval if $a > \pi$. it is also noticed that, as the order of fractional derivative decreases, the critical interval decreases till some fixed value between 0.0468 and 0.0470. Based on numerous results obtained and analyzed in this project, we have been planning further endeavors including impacts of the degeneracy and transport coefficients on quenching solution features [4,7,9,15].

Further, considerations of multidimensional problems may introduce a tremendous amount of difficulties in both analysis and computations. Due to the non-local features of fractional-order differential operators, large and dense matrices are resulted from typical finite difference discretization, since current numerical solutions may depend on solutions on all previous temporal layers. The challenges have led us to several sensitive algorithmic designs and procedures. Highly effective iterative methods, such as the fast multipole and Krylov subspace implementations, have been in our research agendas. Multidimensional and nonlocal fractional quenching problems and operator splitting methods will also be investigated [11,14,27]. Possible applications of fraction quenching-combustion problems in multi-physics and thermal engineering will also been explored in our forthcoming publications.

Acknowledgments

The authors would like to thank the anonymous referees for their time spent and extremely valuable remarks given. Their suggestions have significantly improved the quality and presentation of this paper. The authors also appreciate supports of the American Mathematical Society and National Science Foundation of China.

References

[1] A. Acker, W. Walter, The quenching problem for nonlinear parabolic differential equations, Lect. Notes Math. 564 (1976) 1–12.
[2] H. Cheng, P. Lin, Q. Sheng, R.C.E. Tan, Solving degenerate reaction-diffusion equations via variable step Peaceman–Rachford splitting, SIAM J. Sci. Comput. 25 (2003) 1273–1292.
[3] S. Filippas, J.S. Guo, Quenching profiles for one-dimensional semilinear heat equations, Quart. Appl. Math. 51 (1992) 94–103.
[4] Q. Sheng, Adaptive decomposition finite difference methods for solving singular problems, Front. Math. China 4 (2009) 599–626.
[5] W. Walter, Parabolic differential equations with a singular nonlinear term, Funkcial. Ekvac. 19 (1976) 271–277.
[6] C.Y. Chan, C.S. Chen, A numerical method for semi-linear singular parabolic mixed boundary value problems, Quart. Appl. Math. 47 (1989) 45–57.
[7] J.L. Padgett, The quenching of solutions to time-space fractional Kawarada problems, Comput. Math. Appl. 76 (2018) 1583–1592.
[8] Q. Sheng, A.Q.M. Khaliq, Linearly implicit adaptive schemes for singular reaction-diffusion equations, in: A.V. Wouwer, P. Saucez, W.E. Schiesser (Eds.), Adaptive Methods of Lines, CRC Press, London, New York, 2001, pp. 274–305.
[9] M.A. Beauregard, Numerical approximations to a fractional Kawarada quenching problem, Appl. Math. Comput. 348 (2019) 14–22.
[10] H. Kawarada, On solutions of initial-boundary value problems for $u_t = u_{xx} + \frac{1}{1-u}$, Publ. Res. Inst. Math. Sci. 10 (1975) 729–736.
[11] N. Kavallaris, A. Lacey, C. Nikolopoulos, On the quenching of a nonlocal parabolic problem arising in electrostatic MEMS control, Nonlinear Anal. 138 (2016) 180–206.
[12] W. Huang, Y. Ren, R.D. Russell, Moving mesh partial differential equations (MM-PDEs) based on the equidistribution principle, SIAM J. Numer. Anal. 31 (1994) 709–730.
[13] Q. Sheng, A.Q.M. Khaliq, A compound adaptive approach to degenerate nonlinear quenching problems, Numer. Methods Partial Differential Equations 15 (1999) 29–47.
[14] I. Podlubny, Fractional Differential Equations, first ed., Academic Press, San Diego, CA, 1998.
[15] Y. Xu, Quenching phenomenon in a fractional diffusion equation and its numerical simulation, Int. J. Comput. Math. 95 (2018) 98–113.
[16] L. Zhu, H.X. Rui, Maximum modulus principle estimates for one dimensional fractional diffusion equation, Appl. Math. J. Chinese Univ. 30 (2015) 466–478.
[17] C. Li, A. Chen, Numerical methods for fractional partial differential equations, Int. J. Comput. Math. 95 (2018) 1048–1099.
[18] M.M. Meerschaert, C. Tadjeran, Finite difference approximations for fractional advection-dispersion flow equation, J. Comput. Appl. Math. 172 (2004) 65–77.
[19] Y. Xu, H. Sun, Q. Sheng, On variational properties of balanced central fractional derivatives, Int. J. Comput. Math. 95 (2018) 39–67.
[20] J.W. Mooney, An implicit algorithm for iterating to quenching times in degenerate nonlinear parabolic problems, Dynam. Systems Appl. 5 (1996) 539–551.
[21] Q. Sheng, Y.B. Ge, A numerical endeavor with nonlinear Kawarada equations, Dynam. Systems Appl. 25 (2016) 543–556.
[22] P. Henrici, Discrete Variable Methods in Ordinary Differential Equations, third ed., John Wiley & Sons, New York, NY, 1962.
[23] R.J. LeVeque, Finite Difference Methods for Ordinary and Partial Differential Equations: Steady-State and Time-Dependent Problems, SIAM, Philadelphia, PA, 2007.
[24] A.Q.M. Khaliq, E.H. Twizell, D.A. Voss, On parallel algorithms for semidiscretized parabolic partial differential equations based on subdiagonal Padé approximations, Numer. Methods Partial Differential Equations 9 (1993) 107–116.
[25] J.W. Mooney, A Numerical Method for Accurate Critical Length Estimation in Singular Quenching Problems, in: WSSIAA, vol. 4, 1995, pp. 505–516.
[26] A. Iserles, A First Course in the Numerical Analysis of Differential Equations, second ed., Cambridge University Press, Cambridge, London, 2009.
[27] Q. Sheng, J.L. Padgett, On the stability of a variable step exponential splitting method for solving multidimensional quenching-combustion equations, Springer Proc. Math. Stat. 171 (2016) 155–167.